THE JOURNAL OF PHYSICAL CHEMISTRY B LETTERS

2005, *109,* 3089−3093
Published on Web 02/03/2005

Protein Driven Patterning of Self-Assembled Cubosomic Nanostructures: Long Oriented Nanoridges

Angelina Angelova,*,† Borislav Angelov,‡ Brigitte Papahadjopoulos-Sternberg,§ Claudie Bourgaux,|| and Patrick Couvreur†

CEP, UMR8612 CNRS, University of Paris XI, 5 rue J.B. Clément, F-92296 Châtenay-Malabry, France, Institute of Biophysics, Bulgarian Academy of Sciences, Acad. G. Bonchev Str. Bl.21, BG-1113 Sofia, Bulgaria, Nano Analytical Laboratory, San Francisco, California 94118, U.S.A., and LURE, University of Paris XI, F-91898 Orsay, France

Received: December 20, 2004; In Final Form: January 18, 2005

Self-assembly lipid/protein cubosomic nanostructures are generated at high hydration level (dispersion of 5% lipid only) and examined by freeze-fracture electron microscopy (FF-EM) and synchrotron X-ray diffraction (XRD). The fracture surface of the three-dimensional (3D) soft-matter membranous assembly reveals starlike nanopatterns of oriented 100-nm-long cubosomic nanoridges with lateral periodicity defined by their 21-nm diameters. The average water channel radius in these liquid crystalline cubosomic nanoarchitectures, determined by high-resolution FF-EM and XRD, is 18.0 Å. The protein-directed fragmentation of a diamond-type lipid cubic phase at high hydration can induce 3D patterns of oriented nanoporous building blocks, which are a unique example of tertiary organization of functionalized fluid lipid/water interfaces.

Introduction

Protein functionalization of porous nanostructures[1] of rod and tubule shapes is of current interest for advances in biocatalysis, nanomaterials, and nanofluidics. Recent strategies for preparation of protein-functionalized solid nanorods and nanowires employ template methods for nanowire growth[2] or post-modification of nanotubes by protein anchoring.[3] Mesoporous silica, which effectively entraps proteins,[4] may support the development of porous nanorods and nanowires for biological applications based on highly ordered cubic or hexagonal porous nanostructures.[1,5] While conserving a cubic lattice crystalline order, the self-assembly of nanoporous silicate materials has been associated with very interesting 3D domain patterns and orientations (including dendritic or straight-line and triangular surface morphologies).[6]

In view of the design of biocompatible fluid-phase nanopatterns of rodlike or other nanobuilding-block shapes,[7] lipids[8−17] offer the most natural environment for proteins. Lipid vehicles permit gentle preservation of the protein structure and function in comparison to solid surfaces that may drastically alter the protein conformation. Nonporous lipid nanotubes, being an example of high-aspect-ratio soft-matter nanoparticles, have been obtained by self-assembly.[8−10] Although porous cylindrical cubosomic morphology of fluid nature has been illustrated by Andersson et al.,[18] its experimental realization has been challenging. Such geometry would represent a nanoporous rod with a cubic lattice skeleton (see the double-diamond-type cubic nanochannel system in Figure 1). The challenges with the soft nanoporous materials are (i) how to fragment the continuous liquid crystalline structure into nanometer-size elements and (ii) subsequently proving that the fluid nanoporous organization is preserved in the created nanoscale building blocks.

The bicontinuous cubic lipid/water phases (BCP), and the double diamond (D) structure of the fully hydrated lipid monoolein (MO)[11] in particular, are remarkably organized[13] so that the aqueous phase resides in two intertwined but distinct labyrinthine networks, each exhibiting cubic symmetry, while the lipid bilayer fills the continuous matrix between the two water channel systems (Figure 1). This structure has been a candidate for the preparation of porous spherical nanoparticles termed cubosomes.[19] Despite the fact that protein-involving nanoporous cubosomic vehicles are of nanotechnological interest, the literature does not provide an answer on how to fragment the BCP into rodlike nanoparticles[18] or other desired shapes.[7] How a protein may locate inside the water channels of the dispersed cubosomic nanobuilding blocks is an important related question that also remains without a proper answer. Especially interesting is the case when the size of the protein, to be included into a cubic nanostructure, is larger than the diameter of the water channel (i.e., geometrically incompatible with it). The majority of structural studies of cubic lipid/protein/water phases have been performed at low hydration levels,[12a,13a,14−16] which explains the scarcity of reports on proteocubosome nanoparticle generation in excess aqueous environment. Synchrotron radiation XRD experiments have a potential to overcome the experimental difficulties with highly diluted fluid lipid systems and to collect sufficient signals for determination of their internal nanoperiodicity. Those studies dealt mainly with space group determination, which is not sufficient to describe 3D structures of

* E-mail: Angelina.Angelova@cep.u-psud.fr.
† CEP, UMR8612 CNRS, University of Paris XI.
‡ Bulgarian Academy of Sciences.
§ Nano Analytical Laboratory.
|| LURE, University of Paris XI.

10.1021/jp044216p CCC: $30.25

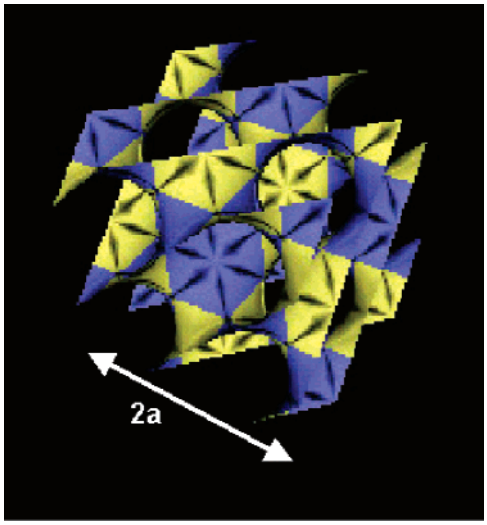

Figure 1. Nanochannel system in double-diamond-type periodic minimal surface. The cubic unit cell dimension is denoted by *a*. The {6, 4} tilling of curved hexagons is shown in yellow and blue.

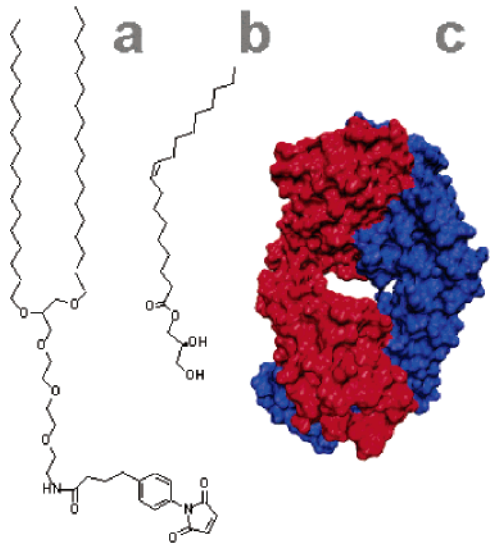

Figure 2. Schematic presentation of the lipids (a) 1-{8-[4-(*p*-maleimidophenyl)butaroylamino]-3,6-dioxaloctyl}-2,3-distearyl glyceryl-DL-ether (MTEG) and (b) 1-monooleoyl-*rac*-glycerol (MO); (c) VMD surface presentation of the protein fragment Fab (volume size 7.9 × 6.7 × 8.5 nm^3) resulting from the PDB structure (1ACY).

cubosomes. The interface structure, the size and shapes of pores, and the enclosed cages should also be investigated at high resolution with such soft porous nanobiostructures.

Here, we demonstrate the protein-induced porous soft-matter nanostructure formation at high hydration level. The created nanostructured fluid is characterized by high-resolution electron microscopy and XRD. Cubosomic nanopatterns were generated upon self-assembly of the mixture of the lipids (1-{8-[4-(*p*-maleimidophenyl)butaroylamino]-3,6-dioxaloctyl}-2,3-distearyl glyceryl-DL-ether (MTEG) and 1-monooleoyl-*rac*-glycerol (MO) in excess solution of a toroidal-shaped protein (immunoglobulin Fab′ fragment) (Figure 2). The protein fragments employed here involve free thiol groups, which are reactive to the polar terminal maleimide group of the MTEG lipid (see details of sample preparation). The interest in including immunoglobulin fragments in nanopattern and nanostructure preparations is determined by the significance of these proteins for immunological biosensor assays as well as for targeted delivery of biomolecules.

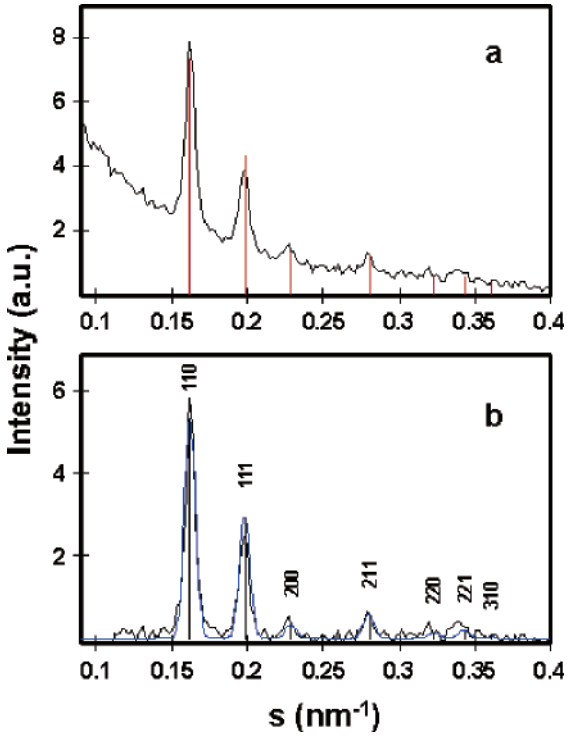

Figure 3. Synchrotron XRD patterns of a self-assembly MO/MTEG/protein cubosomic dispersion at high hydration (95% aqueous phase) recorded at ambient temperature. (a) The integral spectrum that was corrected for instrumental background indicates diffusive scattering. (b) Peak fitting obtained after the subtraction of the diffusive scattering. The indexed Bragg peaks are spaced in the ratio $\sqrt{2}$:$\sqrt{3}$:$\sqrt{4}$:$\sqrt{6}$:$\sqrt{8}$:$\sqrt{9}$:$\sqrt{10}$.... The data fitting, presented with blue peaks, identifies a *Pn*3*m* diamond cubic lattice.

Results and Discussion

This study focuses on the spontaneous 3D self-assembly process of lipid and protein biomolecules with reactive chemical groups at very high dilution of the samples (<5 wt % lipid). It is out of its scope to apply high-energy physical agitation methods that could fragment the lipid/protein assembly into given sizes. The XRD intensities and FF-EM images presented here are apparently associated with the supramolecular structure of organized lipid/protein aggregates, which coexist in equilibrium with large excess of aqueous environment.

Figure 3 shows the synchrotron XRD patterns of the aqueous dispersion of MO/MTEG lipid/protein nanobuilding blocks that were self-assembled upon hydration of 5% lipid phase in the solution of reactive protein fragments (95% aqueous phase). The patterns were treated for background subtraction (a) and peaks fitting (b). We established that the internal periodic organization of the nanoscale building blocks is of the diamond cubic lattice type (space group *Pn*3*m*). The analysis of the X-ray data yielded the following structure parameters: (i) *Pn*3*m* cubic unit cell, $a = 8.75$ nm, and (ii) aqueous channel diameter, $D_w = 3.6$ nm. We recently reported[17a] the structural dimensions of the cubic lattice structure formed, in lack of protein, by self-assembly MO/MTEG lipid mixture (98:2 mol/mol) in 0.1 M NaCl phosphate buffer (pH 7) solution. For a comparison, the cubic *Pn*3*m* unit cell, $a = 8.66$ nm, and the aqueous channel diameter, $D_w = 2.95$ nm, are somewhat smaller in the absence of protein. The differences established here reveal structural modifications due to the presence of protein. However, they hardly suggest that the protein fragments of Fab′ (box size of 7.9 × 6.7 × 8.5 nm^3) are entirely located inside the aqueous channels of the generated D-type cubic nanostructures. Inter-

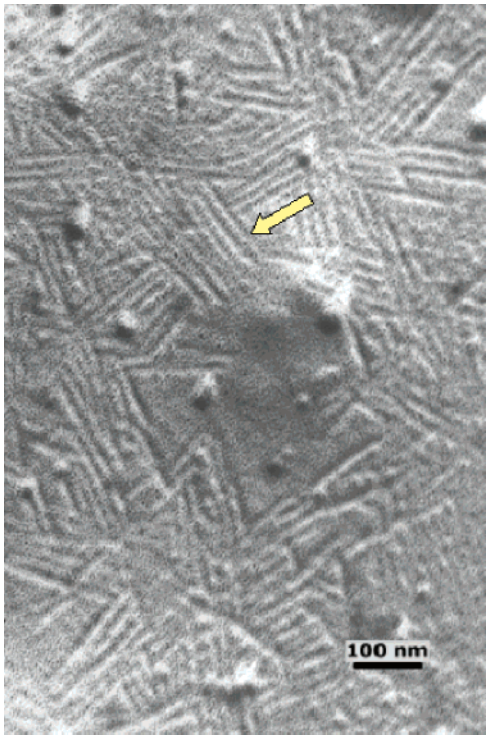

Figure 4. Freeze-fracture electron microscopy image of nanopatterns in cubosomic lipid/protein system generated upon 3D self-assembly of the MO/MTEG mixture in excess solution of immunoglobulin Fab′ protein fragments. The arrow on the crystalline pattern indicates the oriented cubosomic nanoridges, which are magnified in Figure 5.

facial anchoring of proteins at the periphery of the cubosomic nanoassemblies seems very likely. A continued study will be needed to characterize the protein conformation and anchoring in cubosomic structures.

The XRD pattern (Figure 3a), obtained after the subtraction of the instrumental background from the raw data, involves a diffusive scattering characteristic of the diluted sample. It provides evidence that the lipid/protein diffracting structures are dispersed in the aqueous medium. The indexed Bragg peaks are relatively narrow, which suggests that these diffracting structures are large enough in comparison to the unit cell dimension ($a = 8.75$ nm). These conclusions are in agreement with the FF-EM results that demonstrate both the fragmented nature of the diluted sample and the submicron size of a given lipid/protein aggregate.

Figure 4 presents a high-resolution electron microscope image of a freeze-fracture replica of the same MO/MTEG/protein self-assembly system, which is characterized by diamond-type cubic lattice symmetry (Figure 3). The image reveals protein-induced regular patterns of liquid crystalline cubosomic nanoridges. The latter are oriented in starlike networks. The periodicity of the nanoridges within the stars assembly is equal to their diameter (21 nm). The mean nanoridge length varies between 100 and 120 nm. This aspect ratio is typical for all investigated replicas where nanopatterns were found in the diluted sample. The generated lipidic nanoridges are stable in aqueous medium for at least nine months.

The performed nanodissection of the cubosomic lipid/protein 3D aggregate revealed its patterned inner morphology (Figure 4) due to the incorporation of protein macromolecules with reactive groups and the associated intermolecular interactions. The protein-driven propagation of the fracture appears to be favored through arrays of linear nanoridges with discrete orientations, rather than along a particular macroscopic plane

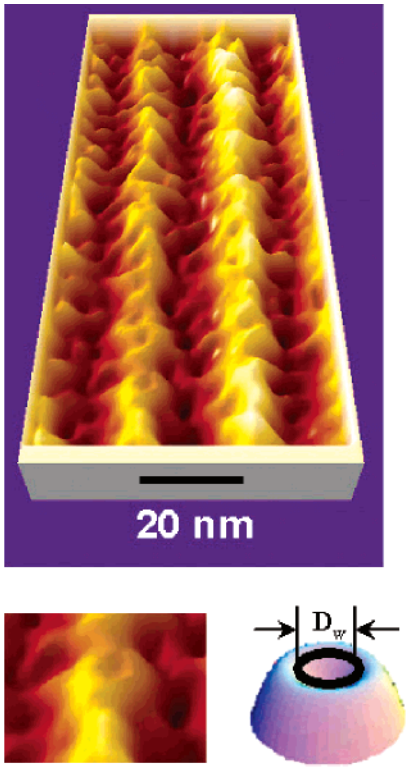

Figure 5. Top: 3D reconstruction of a magnified area of the EM image of the cubosomic nanopattern (see the selection indicated by arrow in Figure 4). Nanopores, characteristic of the fractured aqueous channel system of the BCP, are resolved along the cubosomic nanoridge length. Bottom: Single nanopore with water channel diameter D_w (experiment (left) and modelisation (right)).

with single-crystal appearance.[20] This suggests that the protein−lipid interactions facilitate the fragmentation of the continuous cubosomic structures into nanoscale (~100 nm) patterns.

With the objective to determine the smallest element of the nanoperiodic lipid/protein assembly, we magnified selected areas of the oriented nanopatterns. The magnified FF-EM images were then reconstructed in three dimensions. Figure 5 shows the structure of the nanoridges at high resolution. Noticeably, the bicontinuous cubic organization is preserved along the nanoridge length. Moreover, the nanopattern displays open pores resulting from the water channel system of the D-type lipid/water cubic phase. The open nanopores are visible with a pore diameter around 3.6 nm (see the magnification presented in Figure 5 bottom). The established nanoridge radius, equal to 10.5 nm, suggests that four lipid bilayers and three water channels constitute the cross-section of these excrescences. This is the smallest possible structure-building element of the cubosomic array (a configuration of three lipid bilayers and two water channels cannot form a pore).

The underlying physical mechanism governing the formation of the sophisticated membrane-based nanostructures presented is the lipid bilayer frustration.[21] Our results suggest that the protein fragments, which are geometrically incompatible with the aqueous channel size in the lipid cubic lattice act as supramolecular cutters of the diamond-type structure along certain orientations. As a result, new structures of periodic striated patterns are generated. The protein-directed fragmentation may yield rather small diamond-type cubosomic nanostructures of high aspect ratio (21 nm in diameter and 120 nm in length). A better understanding of the mechanism of nanoridge formation will advance the design of nanostructures in diverse

protein-functionalized nanoporous diamond systems, either soft or solid, including silicates.

In conclusion, the combination of two structural methods (FF-EM and XRD) permitted us to characterize the internal periodic nanochannel structure and the 3D patterning of the cubosomic assembly driven by the incorporation of protein fragments with reactive thiol groups. The smallest building block of the cubosomic nanoridges and the open nanochannels were identified in the EM image of the self-assembly cubosomic pattern.

The presented nanoarchitectures are different with regard to the microwires formed by directed self-assembly of conductive nanoparticles,[22] nanotubule vesicles,[23] neosomes,[24] and previously reported lipid-bilayer-based cubic lattice morphologies.[8−19] The possibility to generate 3D self-assembly lipid/protein nanopatterns is important in the context of the realization of biological interconnections, building blocks in nanodevices, biocatalysis, crystallization of macromolecules on nanotemplates, and targeted protein delivery.

Experimental Section

Materials. The lipids 1-{8-[4-(*p*-maleimidophenyl)butaroylamino]-3,6-dioxaloctyl}-2,3-distearyl glyceryl-DL-ether (MTEG) (purity >99.5%) and 1-monooleoyl-*rac*-glycerol (MO) (purity >99.5%) were purchased by Northern Lipids, Inc., and Sigma, respectively. $F(ab')_2$ fragments of human chrompure immunoglobulin (IgG) were purchased from Jackson ImmunoResearch Laboratories, Inc. Aqueous phase was prepared with 0.1 M NaCl and 10^{-2} M phosphate buffer (pH 7). It was purged with N_2 gas before and during the biochemical preparations. The protein fragmentation by the reagent DTT to yield Fab′ was done according to described procedures.[25,26]

Sample Preparation. Protein/lipid dispersion in excess aqueous phase was obtained upon spontaneous 3D biomolecular self-assembly. Toward this aim, the lipids MO and MTEG were mixed in chloroform at a molar ratio of 98:2, and the solvent was evaporated under nitrogen gas flow during 4 h. The dry lipid mixture was hydrated in excess aqueous phase of the newly generated protein fragments possessing sulfhydryl groups.[25,26] The dispersion contained 5 wt % of lipid phase and 95 wt % of solution phase, which ensured a high hydration level for the lipid/protein cubic phase system. Stable particle dispersion was obtained after repeated vortexing and incubation cycles during 20 min at 37 °C.

X-ray Diffraction Data Analysis. The model of Garstecki Hołyst[27] was used to determine the structural parameters of the diamond cubic lattice structure and the average water channel diameter, D_w. In this model, the lipid bilayer thickness, L, in the cubic lipid phase is estimated from the structural unit cell parameter, a, on the basis of eq 1. The latter relates the intensities in the experimental X-ray patterns with model scattering intensities defined as

$$I_{hkl}^{(\mathrm{mod})}(L) = M_{hkl}\left[F_{hkl}^{S*}\frac{\sin[\alpha_{hkl}\pi(h^2+k^2+l^2)^{1/2}L^*]}{\alpha_{hkl2}\pi(h^2+k^2+l^2)^{1/2}}\right]^2 \qquad (1)$$

where $L^* = L/a$ is the dimensionless lipid layer thickness, F^{S*} is the dimensionless structure factor, M_{hkl} is a multiplicity factor, and α_{hkl} values are correction parameters for particular cubic lattice types.[27] In the Garstecki and Hołyst[27] model, the thickness of the lipid bilayer is assumed to be constant throughout. Having done the fitting for L, D_w was determined from the relationship $D_w = 0.707a - L$. Our fitting algorithm has been described in ref 17b. It is based on the least-squares nonlinear fit using the Levenberg−Marquardt method.

Freeze-Fracture Electron Microscopy. For freeze-fracture electron microscopy,[28] the samples were quenched using the sandwich technique and liquid nitrogen-cooled propane. Using this technique, a cooling rate of 10 000 K/s is reached, avoiding ice crystal formation and artifacts possibly caused by the cryofixation process. The cryofixed samples were stored in liquid nitrogen for less than 2 h before processing. The fracturing process was carried out in JEOL JED-9000 freeze-etching equipment, and the exposed fracture planes were shadowed with Pt for 30 s in an angle of 25−35° and with carbon for 35 s (2 kV/ 60−70 mA, 1×10^{-5} Torr). The replicas produced this way were cleaned with concentrated, fuming HNO_3 for 24 h, followed by repeating agitation with fresh chloroform/methanol (1:1 by vol) at least five times. The replicas cleaned this way were examined with a JEOL 100 CX high-resolution electron microscope.

Image Processing. 3D images of the nanopatterns were obtained by the software *SPIP* (*The Scanning Probe Image Processor*) from Image Metrology (www.imagemet.com). The module *3D Visualization Studio* (version 3.2.10) was used to transform the 2D electron microscope images into 3D images.

Protein Visualization. The immunoglobilin fragment surface was visualized in Figure 2 using the *VMD* software (*Visual Molecular Dynamics*, version 1.8.1; web address www.ks.uiuc.edu/Research/vmd/; see ref 29 for details of *VMD*). The protein atomic coordinates were taken from the Protein Data Bank, PDB ID: 1ACY (ref 30).

References and Notes

(1) (a) Sakamoto, Y.; Koneda, M.; Terasaki, O.; Zhao, D. Y.; Kim, J. M.; Stuky, G.; Shin, H. J.; Ryoo, R. *Nature (London)* **2000**, *408*, 449. (b) Lu, Q.; Gao, F.; Komarneni, S.; Mallouk, T. E. *J. Am. Chem. Soc*. **2004**, *126*, 8650−8651. (c) Wu, Y.; Livneh, T.; Zhang, Y. X.; Cheng, G.; Wang, J.; Tang, J.; Moskovits, M.; Stucky, G. D. *Nano Lett.* **2004**, *4*, 2337−2342. (d) Pradhan, N.; Efrima, S.; *J. Phys. Chem. B* **2004**, *108*, 11964−11970.

(2) (a) Hernández, R.; Richter, L.; Semancik, S.; Stranica, S.; Mallouk, T. E. *Chem. Mater*. **2004**, *16*, 3431−3438.

(3) (a) Nuraje, N.; Banerjee, I. A.; MacCuspil, R. I.; Yu, L.; Matsui, H. *J. Am. Chem. Soc*. **2004**, *126*, 8088−8089. (b) Banerjee, I. A.; Yu, L.; Matsui, H. *Nano Lett*. **2003**, *3*, 283−283.

(4) (a) Ravindra, R.; Zhao, S.; Gies, H.; Winter, R. *J. Am. Chem. Soc*. **2004**, *126*, 12224−12225. (b) Lei, C.; Shin, Y.; Liu, J.; Ackerman, E. J. *J. Am. Chem. Soc*. **2002**, *124*, 11242−3.

(5) (a) Kleitz, F.; Marlow, F.; Stucky, G. D.; Schuth, F. *Chem. Mater*. **2001**, *13*, 3587−3595.

(6) (a) Tian, Z. R.; Liu, J.; Voigt, J. A.; Xu, H.; Mcdermott, M. J. *Nano Lett.* **2003**, *3*, 89−92. (b) Tian, Z. R.; Liu, J.; Xu, H.; Voigt, J. A.; Mckenzie, B.; Matzke, C. M. *Nano Lett.* **2003**, *3*, 179−182.

(7) (a) Zhang, Z. L.; Horsch, M. A.; Lamm, M. H.; Glotzer, S. C. *Nano Lett.* **2003**, *3*, 1341−1346. (b) Zhang, Z. L.; Glotzer, S. C. *Nano Lett.* **2004**, *4*, 1407−1413.

(8) Seddon, J. M.; Templer, R. H. In *Structure and dynamics of membranes*; Lypowsky, R., Sackmann, E., Eds.; Elsevier Science: Amsterdam, The Netherlands, 1995; p 97.

(9) Hafez, I.; Cullis, P. R. *Adv. Drug Delivery Rev.* **2001**, *47*, 139−148.

(10) Lvov, Y. M.; Price, R. R.; Selinger, J. V.; Singh, A.; Spector, M. S.; Schnur, J. M. *Langmuir* **2000**, *16*, 5932−5935.

(11) Hyde, S. T.; Andersson, S.; Ericsson, B.; Larsson, K. *Z.Kristallogr*. **1984**, *168*, 213-219.

(12) (a) Lendermann, J.; Winter, R. *Phys. Chem. Chem. Phys.* **2003**, 1440−1450. (b) Borné, J.; Nylander, T.; Khan, A. *J. Phys. Chem. B* **2002**, *106*, 10492−10500. (c) Funari, S. S.; Rapp, G. *Proc. Natl. Acad. Sci. U.S.A.* **1999**, *96*, 7756−9.

(13) (a) Mariani, P.; Luzzati, V.; Delacroix, H. *J. Mol. Biol*. **1988**, *204*, 165−188. (b) Luzzati, V.; Delacroix, H.; Gulik, A.; GulikKrzywicki, T.; Mariani, P.; Vargas, R. *Lipid polymorphism Membr. Prop., 1997. Curr. Top. Membr*. **1997**, *44*, 3−24. (c) Gruner, S. M. *J. Phys. Chem.* **1989**, *93*, 7562−7570;

(14) Buchheim, W.; Larsson, K. *J. Colloid Interface Sci*. **1987**, *117*, 582.

(15) Ericsson, B.; Larsson, K.; Fontell, K. *Biochim. Biophys. Acta* **1983**, *729*, 23−27.

(16) Leslie, S. B.; Puvvada, S.; Rathna, B. R.; Rudolph, A. S. *Biochim. Biophys. Acta* **1996**, *1285*, 246−254.

(17) (a) Angelova, A.; Ollivon, M.; Campitelli, A.; Bourgaux, C. *Langmuir* **2003**, *19*, 6928−6935. (b) Angelov, B.; Angelova, A.; Ollivon, M.; Bourgaux, C.; Campitelli, A. *J. Am. Chem. Soc*. **2003**, *125*, 7188−7189. (c) Angelov, B.; Ollivon, M.; Angelova, A. *Langmuir* **1999**, *15*, 8225−8234. (d) Angelova, A.; Ionov, R.; Koch, M. H. J.; Rapp, G. *Arch. Biochem. Biophys*. **2000**, *378*, 93−106.

(18) Andersson, S.; Jacob, M.; Lidin, S.; Larsson, K. *Z. Kristallogr*. **1995**, *210*, 315−318.

(19) (a) Gustafsson, J.; Ljusberg-Wahren, H.; Almgren, M.; Larsson, K. *Langmuir* **1996**, *12*, 4611−4613. (b) Spicer, P. T.; Small, W. B., II; Small, W. B.; Lynch, M. L.; Burns, J. L. *J. Nanopart. Res*. **2002**, *4*, 297−311. (c) Spicer, P. In *Marcel Dekker Encyclopedia of Nanoscience and Nanotechnology*; Schwarz, J. A., Contescu, C., Putyera, K., Eds.; Marcel Dekker: New York, 2003.

(20) The latter was reported for cubic lipid phases lacking a protein and for lipid/water compositions with large lipid content (>20 wt % lipid) ((a) Hyde, S.; Andersson, S.; Larsson, K.; Blum, Z.; Landh, T.; Lidin, S.; Ninham, B. W. *The Language of Shape*; Elsevier Science: New York, 1996. (b) Delacroix, H.; Gulik-Krzywicki, T.; Seddon, J. M. *J. Mol. Biol.* **1996**, *258*, 88−103).

(21) (a) Anderson, D. M.; Gruner, S. M.; Leibler, S. *Proc. Natl. Acad. Sci. U.S.A.* **1988**, *85*, 5364−5368. (b) Charvolin, J.; Sadoc, J.-F. In *Micelles, Membranes, Microemulsions, and Monolayers*; Gelbart, W. M., Ben-Shaul, A., Roux, D., Eds.; Springer-Verlag: New York, 1994.

(22) Hermanson, K. D.; Lumsdon, S. O.; Williams, J. P.; Kaler, E. W.; Velev, O. D. *Science* **2001**, *378*, 1082−1086.

(23) Chiruvolu, S.; Warriner, H. E.; Naranjo, E.; Idziak, S. H.; Radler, J. O.; Plano, R. J.; Zasadzinski, J. A.; Safinya, C. R. *Science* **1994**, *266*, 1222−1225.

(24) Sternberg, B.; Moody, M. F.; Yoshioka, T.; Florence, A. T. *Nature (London)* **1995**, 378, 21.

(25) (a) Vikholm, I.; Viitala, T.; Albers, W. M.; Peltonen, J. *Biochim. Biophys. Acta* **1999**, *1421*, 39−52. (b) Ihalainen, P.; Peltonen, J. *Langmuir* **2002**, *18*, 4953−4962.

(26) (a) Renato, B.; Del Rosario, R.; Wahl, L.; Brocchini, S. J.; Lawton, R. G.; Smith, R. H.; *Bioconjugate Chem.* **1990**, *1*, 51−59. (b) Wilbur, D. S.; Stray, J. E.; Hamlin, D. K.; Curtis, D. K.; Robert, L.; Vessella, R. L. *Bioconjugate Chem.* **1994**, *5*, 220−235.

(27) Garstecki, P.; Holyst, R. *Langmuir* **2002**, *18*, 2529−2537.

(28) (a) Sternberg, B.; Hong, K.; Zheng, W.; Papahadjopoulos, D. *Biochim. Biophys. Acta* **1998**, *1375*, 23−35 (b) Torchilin, V. P.; Lukyanov, A. N.; Gao, Z.; Papahadjopoulos-Sternberg, B. *Proc. Natl. Acad. Sci. U.S.A.* **2003**, *100*, 6039−44. (c) Torchilin, V. P.; Levchenko, T. S.; Rammohan, R.; Volodina, N.; Papahadjopoulos-Sternberg, B.; D'Souza, G. G. *Proc. Natl. Acad. Sci. U.S.A.* **2003**, *100*, 1972−7.

(29) Humphrey, W.; Dalke, A.; Schulten, K. *J. Mol. Graphics* **1996**, *14.1*, 33−38.

(30) Ghiara, J. B.; Stura, E. A.; Stanfield, R. L.; Profy, A. T.; Wilson, I. A. *Science*, **1994**, *264*, 82−85.